April 16, 1999

LHC Guide to Parton Distribution Functions and Cross Sections

J. Huston

Department of Physics and Astronomy, Michigan State University, East Lansing, MI 48824, USA

This ATLAS note is intended to serve as a pedagogical guide on the determination of, the proper use of, and the uncertainties of parton distribution functions and their impact on physics cross sections at the LHC. Portions of this note will be placed in the physics TDR.

I. INTRODUCTION

The calculation of the production cross sections at the LHC for both interesting physics processes and their backgrounds relies upon a knowledge of the distribution of the momentum fraction x of the partons in a proton in the relevant kinematic range. These parton distribution functions (pdf's) are determined by global fits to data from deep inelastic scattering (DIS), Drell-Yan (DY), and jet and direct photon production at current energy ranges. Two major groups, CTEQ and MRS, provide semi-regular updates to the parton distributions when new data and/or theoretical developments become available. The newest pdf's, in most cases, provide the most accurate description of the world's data, and should be utlilized in preference to older pdf sets. The newest sets from the two groups are CTEQ5 [1] and MRST [2]. As will be discussed in Section VII, the primary difference between the two pdf's lies in the size the gluon distribution at large x.

This note is intended to serve as a pedagogical summary; the author is a member of CTEQ and apologizes in advance for any bias in that direction.

II. PROCESSES INVOLVED IN GLOBAL ANALYSIS FITS

Lepton-lepton, lepton-hadron and hadron-hadron interactions probe complementary aspects of perturbative QCD (pQCD). Lepton-lepton processes provide clean measurements of $\alpha_s(Q^2)$ and of the fragmentation functions of partons into hadrons. Measurements of deep-inelastic scattering (DIS) structure functions (F_2, F_3) in lepton-hadron scattering and of lepton pair production cross sections in hadron-hadron collisions provide the main source on quark distributions $f^a(x,Q)$ inside hadrons. At leading order, the gluon distribution function g(x,Q) enters directly in hadron-hadron scattering processes with direct photon and jet final states. Modern global parton distribution fits are carried out to next-to-leading (NLO) order which allows $\alpha_s(Q^2), q^a(x,Q)$ and $g(x,Q)$ to all mix and contribute in the theoretical formulae for all processes. Nevertheless, the broad picture described above still holds to some degree in global pdf analyses.

In pQCD, the gluon distribution is always accompanied by a factor of α_s, in both the hard scattering cross sections and in the evolution equations for parton distributions. Thus, determination of α_s and the gluon distribution is, in general, a strongly coupled problem. One can determine α_s separately from e^+e^- or determine α_s and $g(x,Q)$ jointly in a global pdf analysis. In the latter case, though, the coupling of α_s and the gluon distribution may not lead to a unique solution for either. (See for example the discussion in the CTEQ4 paper where good fits were obtained to a global analysis data set, including the inclusive jet data, for a wide range of α_s values. [14] Adjustments to the gluon distribution compensated for the changes in α_s.)

Currently, the world average value of $\alpha_s(M_Z)$ is on the order of 0.118-0.119 [3] The average value from LEP is .121 while the DIS experiments prefer a somewhat smaller value (of the order of 0.116-0.117). Since global pdf analyses are dominated by the high statistics DIS data, they would tend to favor the values of α_s closer to the lower DIS values. The more logical approach is to adopt the world average value of $\alpha_s(M_Z)$ and concentrate on the

determination of the pdf's. This is what both CTEQ and MRS currently do. [1]

The data from DIS, DY, direct photon and jet processes utilized in pdf fits cover a wide range in x and Q. The kinematic 'map' in the (x,Q) plane of the data points used in a recent parton distribution function analyses is shown in Figure 1. The HERA data (H1+ZEUS) are predominantly at low x, while the fixed target DIS and DY data are at higher x. There is considerable overlap, however, with the degree of overlap increasing with time as the statistics of the HERA experiments increases. DGLAP-based NLO pQCD should provide an accurate description of the data (and of the evolution of the parton distributions) over the entire kinematic range shown. At very low x and Q, DGLAP evolution is believed to be no longer applicable and a BFKL description must be used. No clear evidence of BFKL physics is seen in the current range of data; thus all global analyses use conventional DGLAP evolution of pdf's.

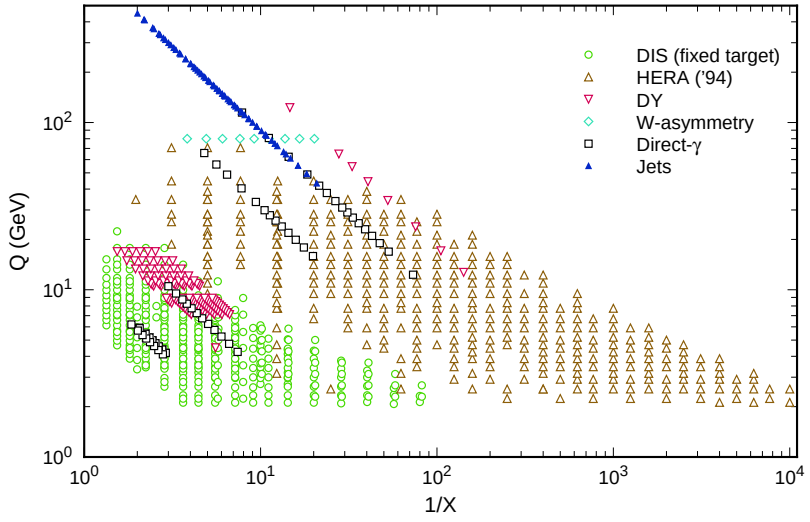

FIG. 1. The kinematic map in the (x,Q) plane of data points used in the CTEQ5 analysis.

---

[1] One can either quote a value of $\alpha_s(M_Z)$ or the value of $\Lambda^{\overline{MS}}$. In the latter case, however, the number of flavors has to be clearly specified, since the value of α_s (and not $\Lambda^{\overline{MS}}$) has to be continuous across flavor thresholds. The range for $\alpha_s(M_Z)$ from .105 to .122 corresponds to $100 < \Lambda_5^{\overline{MS}} < 280\ MeV$ and $155 < \Lambda_4^{\overline{MS}} < 395\ MeV$.

There is a remarkable consistency between the data in the pdf fits and the NLO QCD theory fit to them. Over 1300 data points are shown in Figure 1 and the χ^2/DOF for the fit of theory to data is on the order of 1.

Parton distributions determined at a given x and Q^2 'feed-down' to lower x values at higher Q^2 values. The accuracy of the extrapolation to higher Q^2 depends both on the accuracy of the original measurement and any uncertainty on $\alpha_s(Q^2)$.[2] For the structure function F_2, the typical measurement uncertainty at medium to large x is on the order of $\pm 3\%$. At large x, the DGLAP equation for F_2 can be approximated as $\frac{\partial F_2}{\partial \log\ Q^2} = \alpha_s(Q^2) P^{qq} \otimes F_2$. The effect on the evolution of a world average of α_s and its error ($\alpha_s(M_Z^2) = 0.1175 \pm 0.005$) is shown in Figure 2. [5] There is an extrapolation uncertainty of $\pm 5\%$ in F_2 at high Q^2 ($10^5 GeV^2$) from the given uncertainty in α_s.

---

[2]The evolution can be carried out in either moment space or configuration space. Current programs in use by CTEQ and MRS should be able to carry out the evolution using NLO DGLAP to an accuracy of a few percent over the LHC kinematic range, except perhaps at large x and small x. Note that the theoretical predictions for the W and Z total cross sections at the LHC may have uncertainties of less than 5%. [15] This puts a great demand for the pdf evolution to have accuracies of better than a few percent, since any error on a pdf gets doubled in the cross section calculation. Evolution programs at NNLO may be available at the time of the LHC turnon, but the advantages over NLO evolution may be minimal.

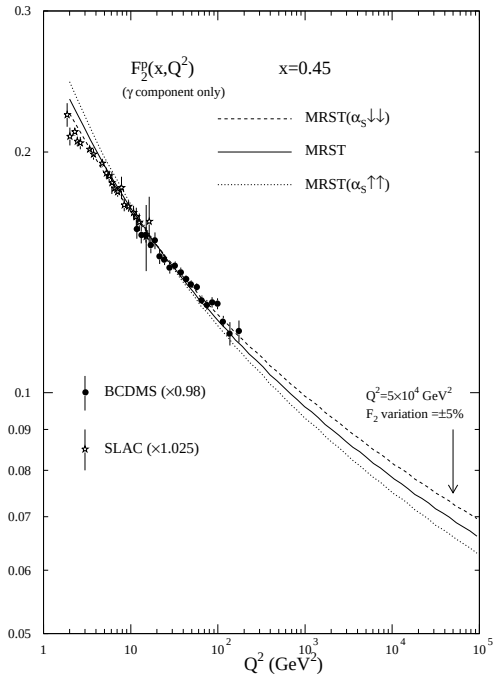

FIG. 2. The extrapolation of the fits at $x = 0.45$ to high Q^2 using the main MRST pdf ($\alpha_s(M_Z) = 0.1175$) and the MRST pdf's corresponding to the upper (.1225) and lower (.1125) range of uncertainty on $\alpha_s(M_Z)$.

Evolution is susceptible to a feed-down on an anomalously large contribution to F_2 near x values of 1. Such a contribution may not be evident in fixed target measurements at low x and low Q^2, but may influence higher Q^2 measurements. Such an example was considered in Reference [6].

For comparison purposes, the kinematics appropriate for the production of a state of mass M and rapidity y at the LHC is shown in Figure 3. [5] For example, to produce a state of mass 100 GeV and rapidity 2 requires partons of x values .05 and .001 at a Q^2 value of $1X10^4\ GeV^2$. Also shown in the figure is another view of the kinematic coverage of the fixed target and HERA experiments used in pdf fits.

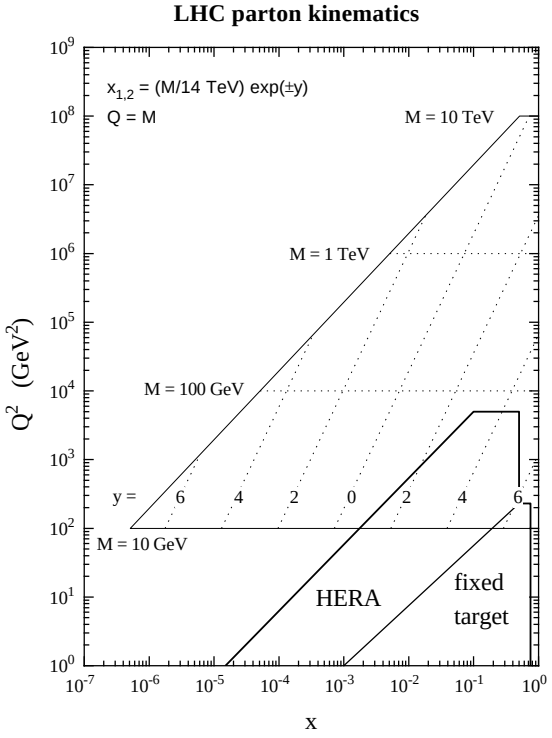

FIG. 3. A plot of LHC parton kinematics in (x, Q^2) space. Also shown are the reach of fixed target and HERA experiments.

III. PARAMETERIZATIONS AND SCHEMES

A global pdf analysis carried out at next-to-leading order needs to be performed in a specific renormalization and factorization scheme. The evolution kernels are in a speciic scheme and to maintain consistency, any hard scattering cross section calculations used for the input processes or utilizing the resulting pdf's need to have been implemented in that same renormalization scheme. Almost universally, the $\overline{MS}$ scheme is used; pdf's are also available in the DIS scheme, a fixed flavor scheme (a la GRV [7]) and several schemes that differ in their specific treatment of the charm quark mass. The choices for the latter are: zero-mass-charm parton, no charm parton (the fixed flavor scheme above) and massive-charm partons. The emergence of quantitative data on charm and bottom production requires a

more precise definition of the scheme used to treat the heavy flavors.

In the standard CTEQ5 pdf's, the conventional 3-4-5 ("variable") flavor scheme with zero-mass-charm partons is used; for specific applications involving identified charm in the final states, it is better to adopt the more general scheme using non-zero charm mass hard cross sections for the relevant charm production process. In the CTEQ5HQ set, the heavy quark masses are explictly taken into account in the pdf fits while in the CTEQ5F3 set (the fixed flavor scheme) , the charm and bottom quarks are treated as heavy particles and not as partons.

It is also possible to use only leading-order matrix element calculations in the global fits which results in leading-order parton distribution functions. Such pdf's are preferred when leading order matrix element calculations (such as Monte Carlo programs like Herwig [8] and Pythia [9]) are used. The differences between LO and NLO pdf's, though, are formally NLO; thus, the additional error introduced by using a NLO pdf with Herwig rather than a LO pdf, for example, should not be significant, in principle, and NLO pdf's can be used when no LO alternatives are available. The accuracy of current DIS/DY data is such that the χ^2 values for LO fits are noticeably worse than those from the NLO fits. The data are sensitive to the differences between LO and NLO matrix elements.

All global analyses use a generic form for the parameterization of both the quark and gluon distributions at some reference value Q_o:

$$F(x, Q_o) = A_o x^{A_1} (1-x)^{A_2} P(x; A_3, ...)$$

The reference value Q_o is usually chosen in the range of 1-2 GeV. The parameter A_1 is associated with small-x Regge behavior while A_2 is associated with large-x valence counting rules. In some pdf fits, A_1^{gluon} has been tied to $A_1^{seaquark}$; in more recent fits like CTEQ4, CTEQ5 and MRST, the two small x exponents are allowed to vary independently. The current statistical power of the low x and Q^2 DIS data from HERA warrants the separation.

The first two factors, in general, are not sufficient to describe either quark or gluon distributions. The term $P(x; A_3, ...)$ is a suitable chosen smooth function, depending on one or more parameters, that adds more flexibility to the pdf parameterization. In general, both

the number of free parameters and the functional form can have an influence on the global fit. For example, the MRS group traditionally uses $P_{MRS}(x; A_3, A_4) = 1 + A_3\sqrt{x} + A_4 x)$. The CTEQ3 pdf used $P_{CTEQ3} = 1 + A_3 x$ while CTEQ2, CTEQ4 and CTEQ5 all use the more general form $P_{CTEQ2,4,5} = 1 + A_3 x^{A_4}$. The flexibility in the latter form, for example, makes possible the larger gluon at high x observed in the CTEQ4HJ pdf.

Although the pdf's determined from global analyses should, in principle, be universal, in practice they could depend on the choice of data sets, and in particular on the choice of Q_{cut} values that specify the minimum hard physical scale $(Q, p_T, ..)$ required for data points to be included in the fit. If NLO QCD is truly applicable in the kinematic region of the data, the parton distributions should be insensitive to the value of Q_{cut}. This point has to be investigated phenomenologically for each process. For a discussion of this point, see Reference [10].

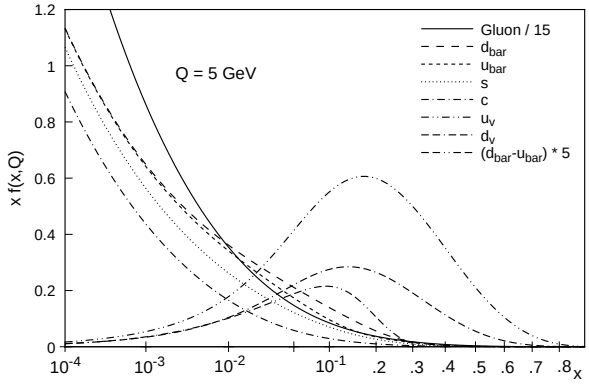

FIG. 4. The parton distributions from the CTEQ5 set plotted at a Q value of 5 GeV.

The pdf's made available to the world from the global analysis groups can either be in a form where the x and Q^2 dependence is parameterized, or the pdf's for a given x and Q^2 range can be interpolated from a grid that is provided. Both techniques should provide an accuracy on the output pdf distributions on the order of a few percent for the LHC kinematic range, although this is a point which probably should be investigated in more detail.

The parton distributions from the recent CTEQ pdf release are plotted in Figure 4 at a Q value of 5 GeV. The gluon distribution is dominant at x values of less than .01 with the

valence quark distributions dominant at higher x.

IV. EVOLUTION IN TIME AND Q^2

As discussed in the introduction, the MRS and CTEQ groups provide semi-regular updates to their parton distributions as new data and/or theory becomes available. The latest parton distributions are the most accurate and should be used in preference to previous pdf's. However, in some cases calculations using older pdf's are necessary; for example, none of the more recent pdf's are implemented in Pythia, and most comparisons in the ATLAS TDR are made with the CTEQ2L pdf (the default pdf in Pythia).

A comparison of the CTEQ1M [11], CTEQ2M [12], CTEQ3M [13] and CTEQ4M [14] parton distributions are shown in Figures 5, 6, and 7 for the case of the valence up quark, up sea quark and gluon distributions, respectively, at a Q value of 5 GeV.

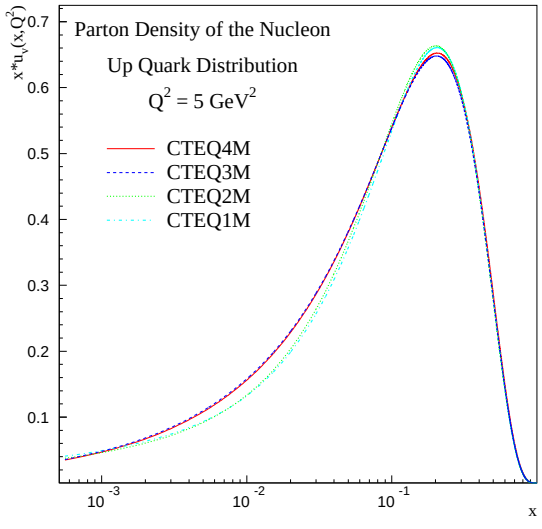

FIG. 5. The valence u quark parton distributions from the CTEQ1-4 sets plotted at a Q^2 value of 5 GeV^2.

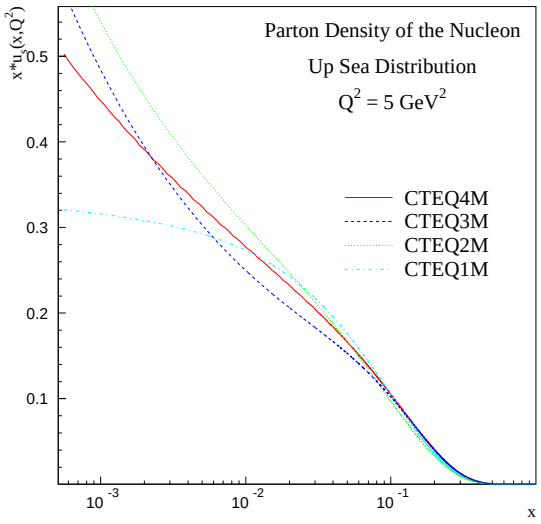

FIG. 6. The up sea quark parton distributions from the CTEQ1-4 sets plotted at a Q^2 value of 5 GeV^2.

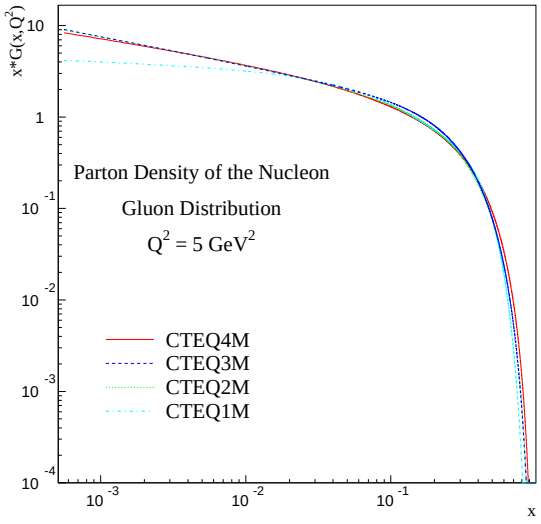

FIG. 7. The gluon parton distributions from the CTEQ1-4 sets plotted at a Q^2 value of 5 GeV^2 using a logarithmic scale in x.

There is little change in the valence up quark distribution while the CTEQ2-4 up quark

sea distributions are substantially steeper than that of CTEQ1, reflecting the influence of the HERA data. A similar effect is seen with the gluon distribution.

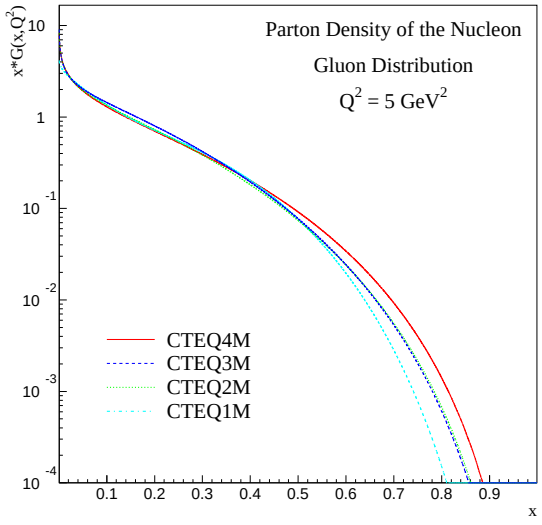

FIG. 8. The gluon parton distributions from the CTEQ1-4 sets plotted at a Q^2 value of 5 GeV^2 using a linear scale in x.

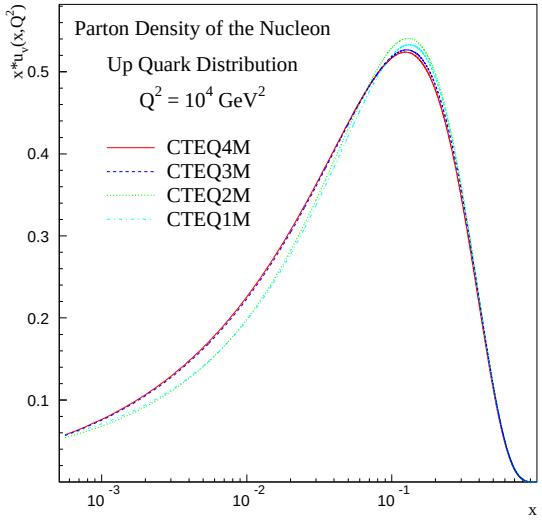

FIG. 9. The up quark valence parton distributions from the CTEQ1-4 sets plotted at a Q^2 value of 10^4 GeV^2.

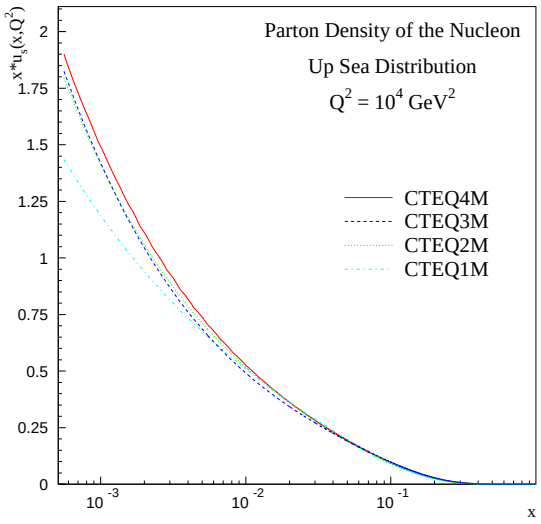

FIG. 10. The up sea quark parton distributions from the CTEQ1-4 sets plotted at a Q^2 value of $10^4\ GeV^2$.

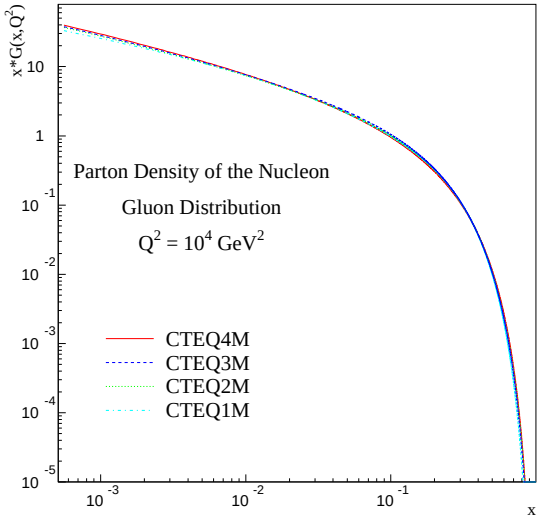

FIG. 11. The gluon parton distributions from the CTEQ1-4 sets plotted at a Q^2 value of $10^4\ GeV^2$ using a logarithmic scale in x.

In Figure 8, the CTEQ1-4 gluon distributions are plotted on a linear scale in x to accentuate the high x region. The tendency has been for the gluon to become larger with

time at high x. As will be seen later, large x is a region where the gluon distribution is fairly unconstrained.

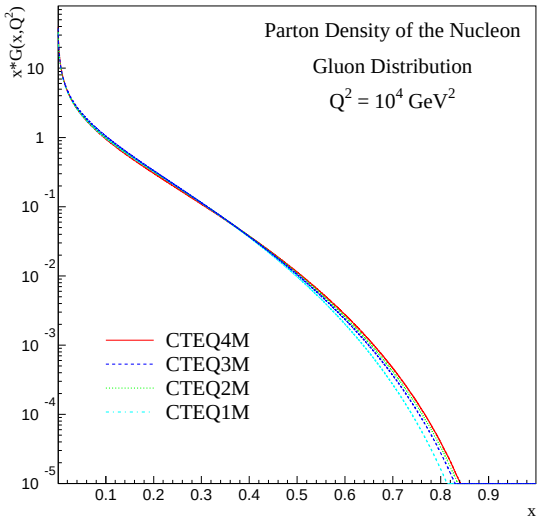

FIG. 12. The gluon parton distributions from the CTEQ1-4 sets plotted at a Q^2 value of $10^4\ GeV^2$ using a linear scale in x.

The same distributions are shown in Figures 9, 10, 11 at a larger Q^2 value of $10^4\ GeV^2$. Evolution has evened out many of the differences observed at lower Q^2 values. A Q^2 value of $10^4\ GeV^2$ corresponds to a mass scale at the LHC of about 100 GeV.

The effects of evolution are examined in more detail in Figures 13, 14 and 15 where the gluon, up valence and up sea quark distributions are plotted at Q^2 values of 2, 10, 50, 10^4 and $10^6 GeV^2$. There are two interesting features that can be noted. Most of the evolution takes place at low Q^2 and there is little evolution for x values in the vicinity of 0.1. In contrast, at an x value of 0.5, the gluon distribution decreases by a factor of approximately 30 from the lowest to the highest Q^2 value.

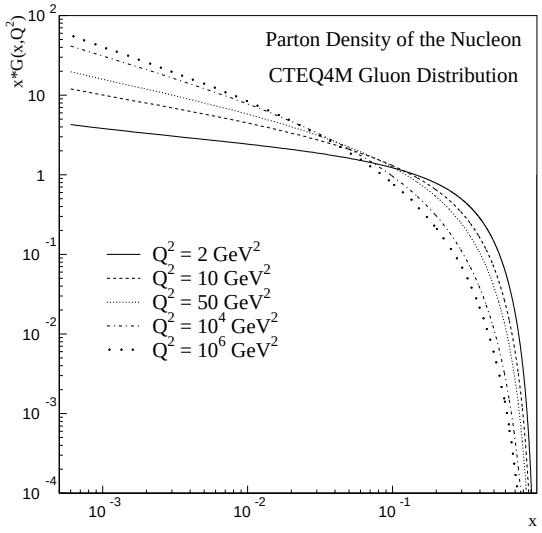

FIG. 13. The gluon parton distribution from CTEQ4M shown at 5 different Q^2 scales.

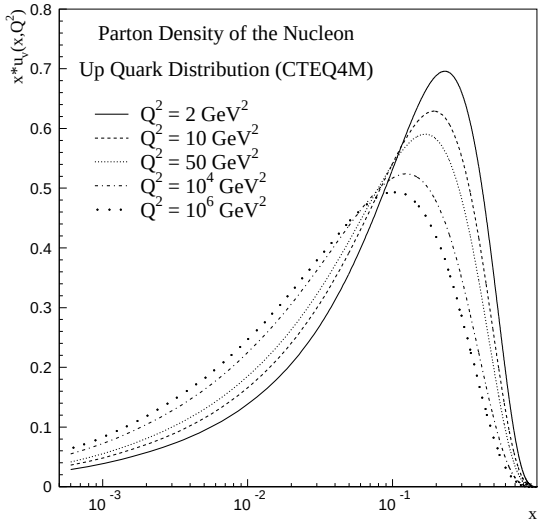

FIG. 14. The u valence quark parton distribution from CTEQ4M shown at 5 different Q^2 values.

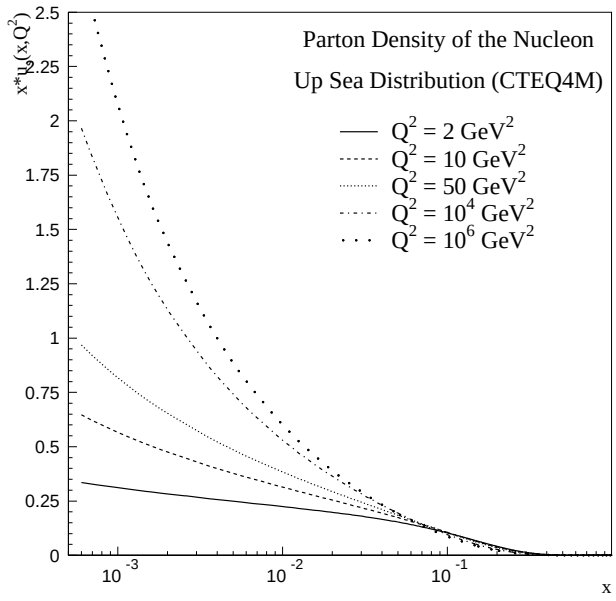

FIG. 15. The u sea quark parton distribution from CTEQ4M shown at 5 different Q^2 values.

V. NLO AND LO PDF'S

As mentioned previously, pdf's are also available from leading order fits to the same data sets used in the NLO fits. For many hard matrix elements for processes used in the global analysis, there exist K factors (NLO/LO) signficantly different from unity. Thus, one expects there to be comparable differences of the LO parton distributions from the NLO ones. A comparison of the LO and NLO gluon, u valence quark and u sea quark distributions for the CTEQ4 set is shown in Figures 16, 17 and 18 at a Q^2 value of 5 GeV^2 and in Figures 19, 20 and 21 at a Q^2 value of 10^4 GeV^2.

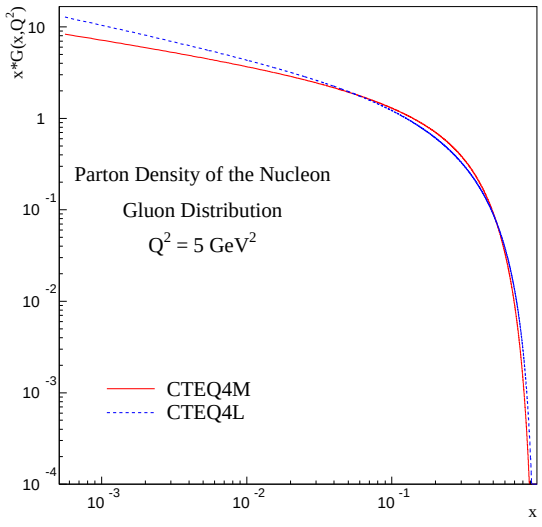

FIG. 16. A comparison of the gluon parton distributions from the CTEQ4 LO and NLO sets plotted at a Q^2 value of 5 GeV^2.

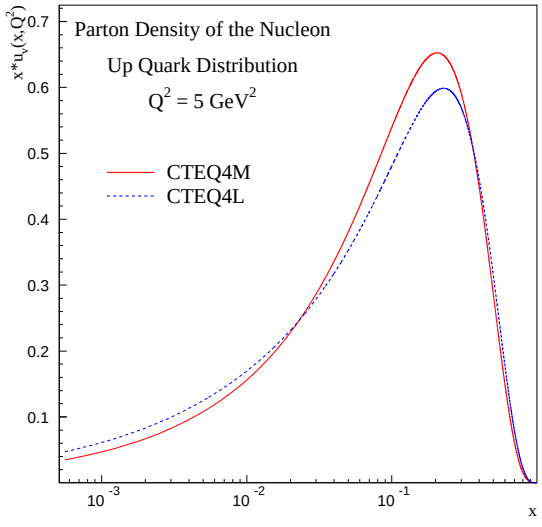

FIG. 17. A comparison of the the u valence quark distributions from the CTEQ4 LO and NLO sets plotted at a Q^2 value of 5 GeV^2.

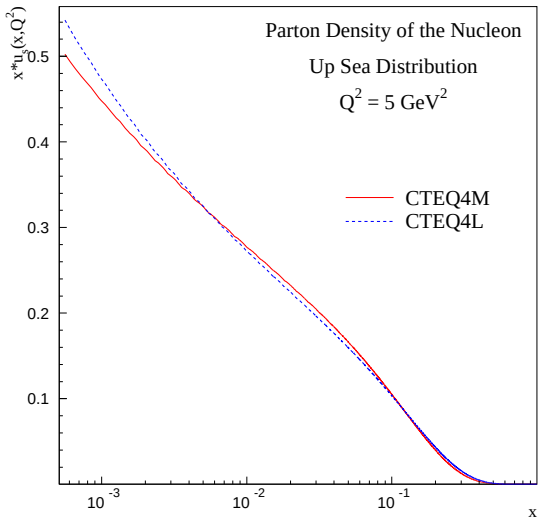

FIG. 18. A comparison of the u sea quark distributions from the CTEQ4 LO and NLO sets plotted at a Q^2 value of 5 GeV^2.

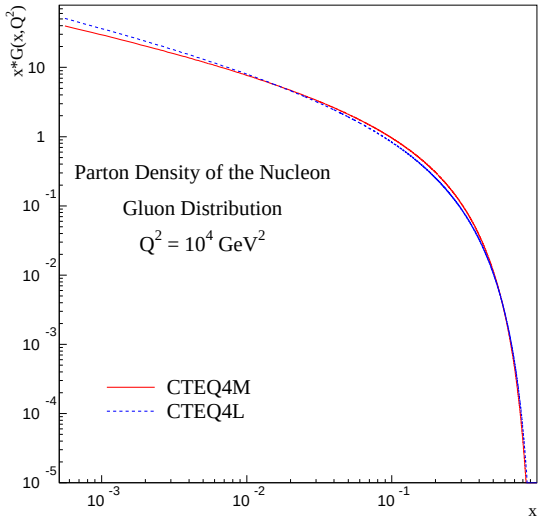

FIG. 19. A comparison of the the gluon parton distributions from the CTEQ4 LO and NLO sets plotted at a Q^2 value of 10^4 GeV^2.

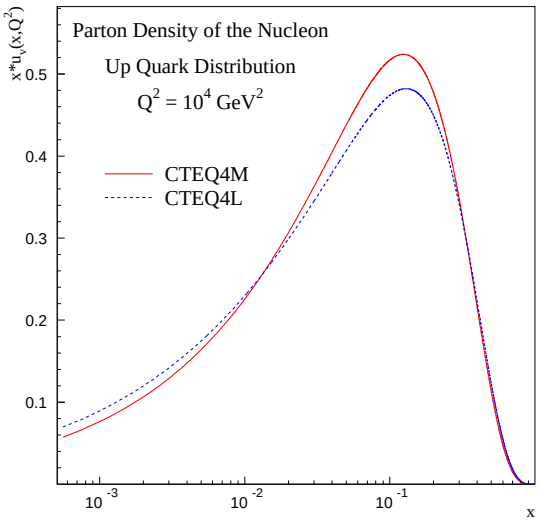

FIG. 20. A comparison of the u valence quark parton distributions from the CTEQ4 LO and NLO sets plotted at a Q^2 value of $10^4\ GeV^2$.

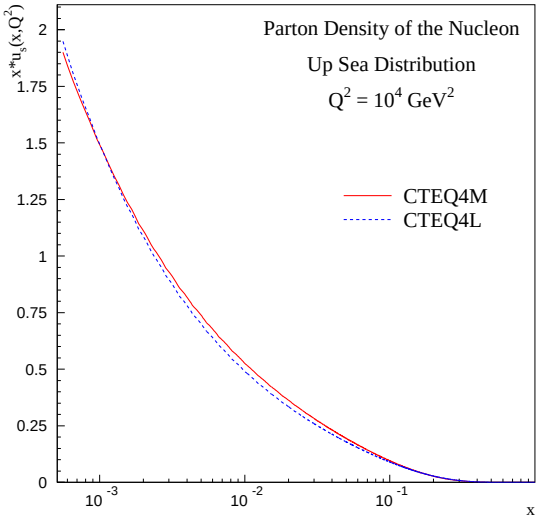

FIG. 21. A comparison of the the u sea quark parton distributions from the CTEQ4 LO and NLO sets plotted at a Q^2 value of $10^4\ GeV^2$.

The differences between NLO and LO parton distributions are not that large for many pdf's in many regions of x and again tend to shrink at higher Q^2.

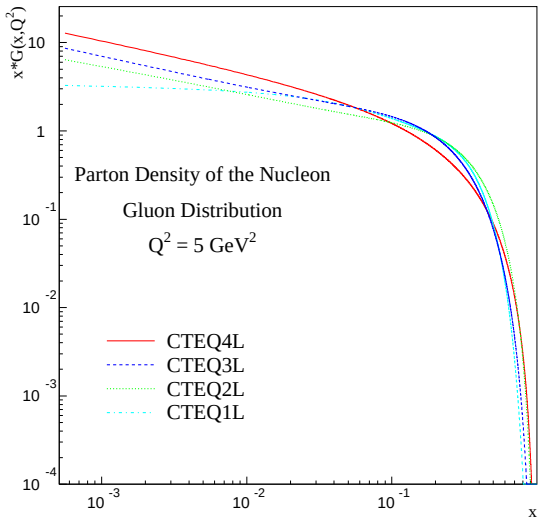

FIG. 22. The gluon parton distributions from the CTEQ1-4 LO sets plotted at a Q^2 value of 5 GeV^2.

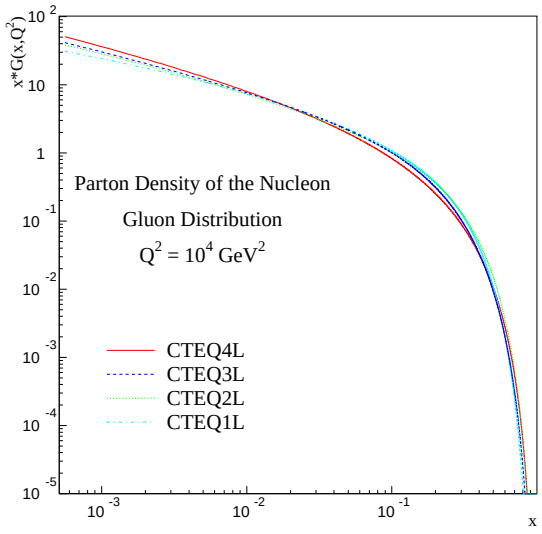

FIG. 23. The gluon parton distributions from the CTEQ1-4 LO sets plotted at a Q^2 value of 10^4 GeV^2.

The same evolution (in time and Q^2) for the gluon distribution in the LO pdf's is shown in Figure 22 and Figure 23. It is interesting to note that the gluon distribution in the kinematic region appropriate for production of a light Higgs has not changed appreciable from CTEQ2L to CTEQ4L.

VI. UNCERTAINTIES ON PDF'S

In addition to having the best estimates for the values of the pdf's in a given kinematic range, it is also important to understand the allowed range of variation of the pdf's, i.e. their uncertainties. The conventional method of estimating parton distribution uncertainties is to compare different published parton distributions. This is unreliable since most published sets of parton distributions (for example from CTEQ and MRS) adopt similar assumptions and the differences between the sets do not fully explore the uncertainties that actually exist. Ideally, one might hope to perform a full error analysis and provide an error correlation matrix for all the parton distributions. (See for example, Ref. [16].) This goal is an admirable one but is difficult to carry out for two reasons. Experimentally, only a subset of the experiments usually involved in global analyses provide correlation information on their data sets in a way suitable for the analysis. Even more important, there is no established way of quantifying the theoretical uncertainties for the diverse physical processes that are used and uncertainties due to specific choices of parameterizations. Both of these are highly correlated. One possibility that has been explored [17] is to invoke only the DIS process, to use only DIS data with the needed correlation information, and to use only those data points at high Q^2 where the theoretical uncertainties are expected to be small. Since these limitations do not take into account the constraints provided by the wide range of data/processes that are thrown away, the uncertainties are clearly unrealistic.

The sum of the quark distributions ($\Sigma(q(x) + \overline{q}(x))$ is, in general, well-determined over a wide range of x and Q^2. As stated above, the quark distributions are predominantly determined by the DIS and DY data sets which have large statistics, and systematic errors

in the few percent range ($\pm 3\%$ for $10^{-4} < x < 0.75$). Thus the sum of the quark distributions is basically known to a similar accuracy. The individual quark flavors, though, may have a greater uncertainty than the sum. This can be important, for example, in predicting distributions that depend on specific quark flavors, like the W asymmetry distribution [18] and the W rapidity distribution.

Information on the $\overline{d}$ and $\overline{u}$ distributions comes, at small x, from HERA and at medium from fixed target DY production on H_2 and D_2 targets. It is now well-established [19,20] that the $\overline{d}$ and $\overline{u}$ distributions are not the same. This can be observed, for example, in the plot of the $\overline{d}/\overline{u}$ distribution in Figure 24. The difference between the CTEQ4M and CTEQ5M pdf's is due primarily to the influence of the data from the E866 experiment. It is worth noting that our detailed knowledge of $\overline{d}/\overline{u}$ is limited primarily to the x region (.03-.35) covered by E866.

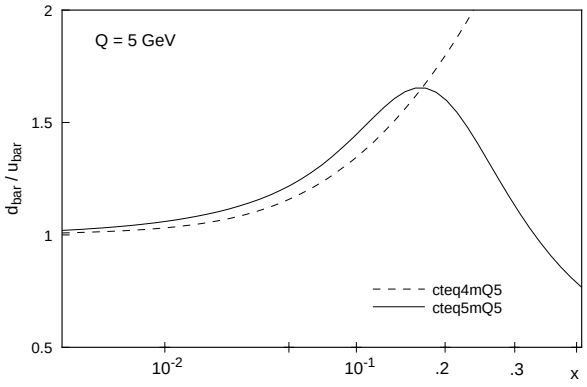

FIG. 24. A plot of the ratio of the $\overline{d}$ and $\overline{u}$ distributions as a function of x evaluated at Q=5 GeV for the CTEQ4M and CTEQ5M pdf's.

The strange quark sea is determined from dimuon production in ν DIS (CCFR [21]), with the strange quark distribution $(s + \overline{s})$ being approximately 1/2 $(\overline{u} + \overline{d})$. The charm and bottom quark distributions are calculated perturbatively from gluon splitting for given masses of m_c and m_b. (See also the previous discussion on schemes.)

Current information on d/u at large x comes from fixed target DY productin on H_2 and D_2 and the lepton asymmetry in W production at the Tevatron. In the CTEQ5 and

MRST fits, the NMC D_2/H_2 data are used to constrain the large x d quark distribution in this way. Bodek and Yang have argued that the D_2 data need to be corrected for nuclear binding effects, which would lead to a larger d/u ratio at large x (and thus a larger d quark distribution as the u quark distribution is well-determined from DIS). [22] The larger d quark distribution would lead to an increase in the high E_T Tevatron jet cross section of about 10%. A similar excess would be expected for high E_T jet production at the LHC.

The largest uncertainty of any parton distribution, however, is that on the gluon distribution. The gluon distribution can be determined indirectly at low x by measuring the scaling violations in the quark distributions ($\partial F_2/\partial log Q^2$), but a direct measurement is necessary at moderate to high x. Direct photon production has long been regarded as potentially the most useful source of information on the gluon distribution with fixed target direct photon data, especially from the experiment WA70 [4], being used in a number of global analyses. However, as will be discussed in Section VII, there are a number of theoretical complications with the use of direct photon data. Possible sources of information on the gluon distribution and their approximate x range are shown in Figure 25 [5], along with a plot of the MRST gluon pdf.

The LHC is essentially a gluon-gluon collider and many hadron-collider signatures of physics both within and beyond that Standard Model involve gluons in the initial state. Thus, it is important to estimate the theoretical uncertainty due to the uncertainty in the gluon distribution.

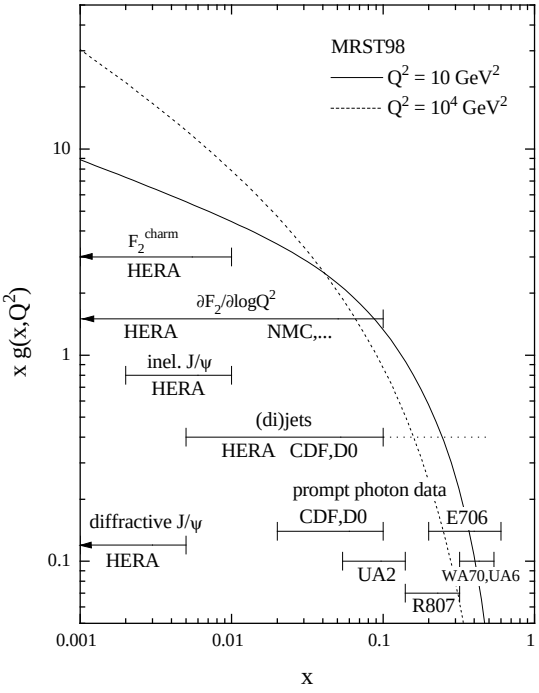

FIG. 25. Sources of information on the gluon distribution.

The momentum fraction of the proton carried by quarks is determined very well from DIS data; at a Q_o value of 1.6 GeV, in the CTEQ4 analysis for example, the momentum fraction carried by quarks is 58% with an uncertainty of $\pm 2\%$. Thus, the momentum fraction carried by gluons is 42% with a similar uncertainty. This constraint is important; if the gluon distribution increases in one x range, momentum conservation forces it to decrease in another x range. The fraction of the proton momentum taken by gluons in a given x range is shown in Table I below. The distribution of gluon momentum fraction is also seen shown in Figure 26. The shift of the gluons to lower x values with increasing Q^2 is evident. The fraction of parton momentum taken by gluons also increases with increasing Q^2.

X Bin	Momentum fraction
10^{-4} to 10^{-3}	0.6%
10^{-3} to 0.01	3%
0.01 to 0.1	16%
0.1 to 0.2	10%
0.2 to 0.3	6%
0.3 to 0.5	5%
0.5 to 1.0	1%

TABLE I. The momentum fraction carried by gluons in a a given x bin at a Q value of 5 GeV.

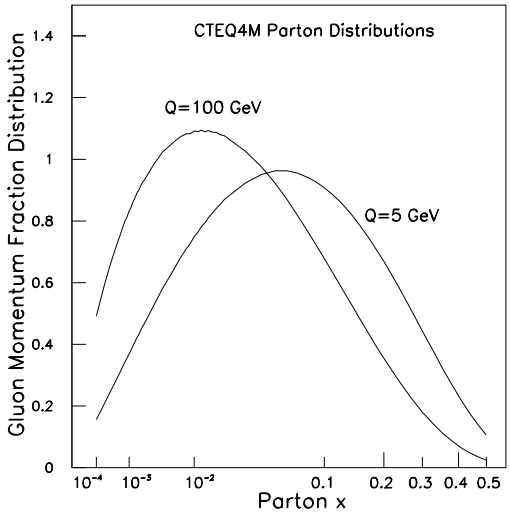

FIG. 26. The fraction of momentum taken by gluons of a given x value for Q = 5 GeV and Q = 100 GeV.

Thus, if the gluon flux in the x range from 0.01 to 0.3 were to decrease by 20%, the gluon flux would have to increase by a fairly dramatic amount in the other x ranges to compensate. For example, if this compensation were to come in the high x region, the gluon distribution would have to double.

An alternative approach, to those described above, for estimating the uncertainty on the gluon distribution is to systematically vary the gluon parameters in a global analysis and then look for incompatibilities with the data sets that make up the global analysis database. This study has been recently carried out by CTEQ using only DIS and Drell-Yan data where the theoretical and experimental systematic errors are under good control. [23] The CTEQ4 parameterization for the gluon distribution $A_o x^{A1}(1-x)^{A2}(1+A_3 x^{A4})$ was used for this study. The CTEQ4M value of α_s (0.116) was used; the values of A_1, A_2, A_3 and A_4 were systematically varied, each time refitting the other gluon and quark parameters. The gluon pdf's that do not clearly contradict any of the data sets used are shown in Figure 27.[3]

[3]All of the parton distribution functions shown in Figure 27 are available from the CTEQ web

Except at larger values of $x(x > 0.2 - 0.3)$, the variation in the gluon distributions is less than 15% at low values of Q, decreasing to less than 10% at high values. [4] Note that the DIS and DY datasets used in this analysis do not provide any strong constraints on the gluon distribution at high values of x. This study used the CTEQ4 value of α_s. If α_s is varied in the range from 0.113 to 0.122, the gluon distribution varies by 3% for $x < 0.15$.

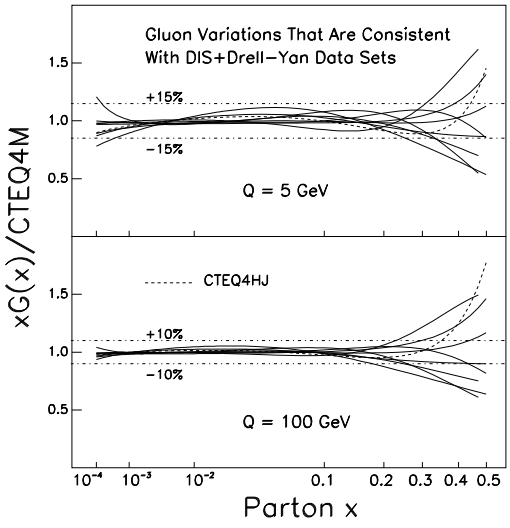

FIG. 27. The ratio of gluon distributions consistent with the DIS and DY data sets to the gluon distributions from CTEQ4M. The gluon distribution from CTEQ4HJ is also shown for comparison.

In order to assess the range of predictions on physics cross sections, it is more important to know the uncertainties on the gluon-gluon and gluon-quark luminosity functions at the appropriate kinematic region (in $\tau = x_1 x_2 = \hat{s}/s$) rather than on the parton distributions themselves. Therefore it is useful to define the relevant integrated parton-parton luminosity functions. The gluon-gluon luminosity function can be defined as:

$\tau dL/d\tau = \int_\tau^1 G(x,Q^2)G(\tau/x,Q^2)dx/x$

---

site, http://www.phys.psu.edu/ cteq/.

[4] As noted earlier, evolution is the great equalizer for parton distributions.

This quantity is directly proportional to the cross section for s-channel production of a single particle and it also gives a good estimate for more complicated production mechanisms. In Figure 28 is shown the range of allowed gluon-gluon luminosities (normalized to the CTEQ4M values) for the variations discussed above. Here, Q^2 is taken to be τs, which naturally takes the Q^2 dependence of the gluon distribution into account as one changes $\sqrt{\tau}$. The top region is for the LHC and the bottom is for the Tevatron. The region of production of a 100-140 GeV Higgs at the LHC is indicated; it lies in the region where the range of variation is $\pm 10\%$. Above an x value of 0.1, the allowed variation grows dramatically (we are squaring the variation shown in Fig. 27) ; this indicates the need for more information about the gluon distribution at large x than provided by the DIS and DY data sets used in this analysis.

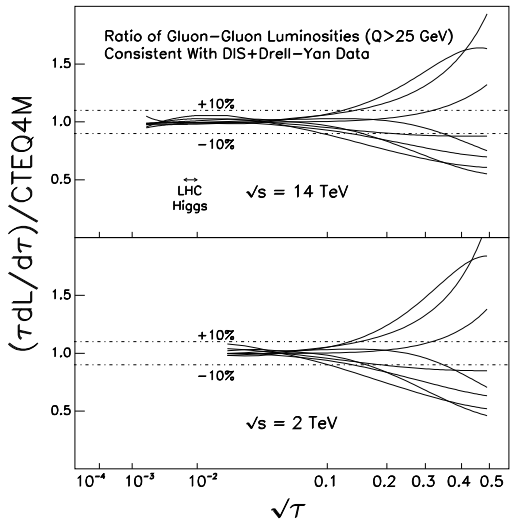

FIG. 28. The rato of integrated gluon-gluon luminosities compared to CTEQ4M is shown as a function of $\sqrt{\tau}$. Shown are examples that are consistent with the DIS+DY data sets used in the fits.

In analogy with the discussion of gluon-gluon luminosities, one can also study the gluon-quark luminosity (again normalized to the CTEQ4M result). The gluon-quark luminosity variations are shown in Figure 29 as a function of $\sqrt{\tau}$ for both the LHC and the Tevatron.

(In the plots below, the quark distributions are taken to have no uncertainty; this is not totally unreasonable since the uncertainty on the gluon is considerably larger.)

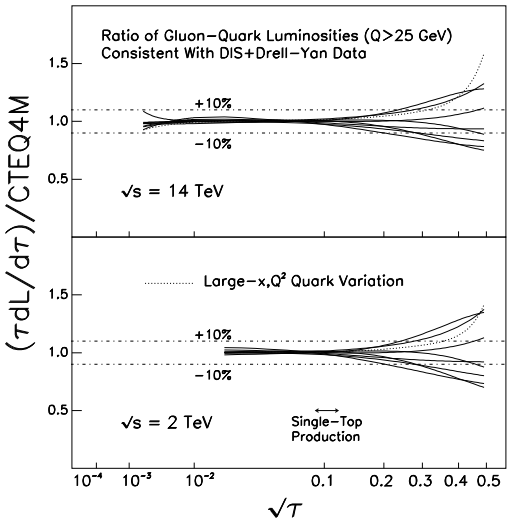

FIG. 29. The ratio of integrated gluon-quark luminosities compared to CTEQ4M is shown as a function of $\sqrt{\tau}$. The examples shown are those consistent with the DIS+DY data sets used in the fits.

The uncertainties on the parton-parton luminosities, as a function of $\sqrt{\tau}$, is summarized in Table II below:

$\sqrt{\tau}$ range	gluon-gluon	gluon-quark
< 0.1	$\pm 10\%$	$\pm 10\%$
$0.1 - 0.2$	$\pm 20\%$	$\pm 10\%$
$0.2 - 0.3$	$\pm 30\%$	$\pm 15\%$
$0.3 - 0.4$	$\pm 60\%$	$\pm 20\%$

TABLE II. The parton-parton luminosity uncertainty as a function of $\sqrt{\tau}$.

VII. DIRECT PHOTONS AND JETS IN GLOBAL FITS

A. Direct Photons

As mentioned previously, direct photon production has long been viewed as an ideal vehicle for measuring the gluon distribution in the proton. The quark-gluon Compton scattering subprocess ($gq \rightarrow \gamma q$) dominates photon production in all kinematic regions of pp scattering, as well as for low to moderate values of parton momentum fraction x in $\overline{p}p$ scattering. As mentioned in the previous section, the gluon distribution is relatively well constrained at low $x(x < 0.1)$ by DIS and DY data, but less so at higher x. Consequently, fixed target direct photon data have been incorporated in several modern global parton distribution function analyses with the hope of providing a major constraint on the gluon distribution at moderate to high x.

A pattern of deviations of direct photon data from NLO predictions has been observed [24], however, with the deviations being particularly striking for the E706 experiment. The origin of the deviations lies in the effects of initial state soft gluon radiation, or k_T. [5] Direct evidence of this k_T has long been evident from Drell-Yan, diphoton and heavy quark measurements. The values of $< k_T >$/parton for these processes vary from 1 GeV/c at fixed target energies to 3-4 GeV/c at the Tevatron Collider. The growth is approximately logarithmic with center of mass energy as can be seen in Figure 30. (The value expected at the LHC for relatively low mass states (30-40 GeV/c^2) is in the range of 6.5-7.0 GeV/c; the $\langle k_T \rangle$ (due to the effects of soft gluon radiation) at a given $\sqrt{s}$ should increase logarithmically with the mass of the state.

---

[5] I should add that this view is not universally held; see for example Reference [25].

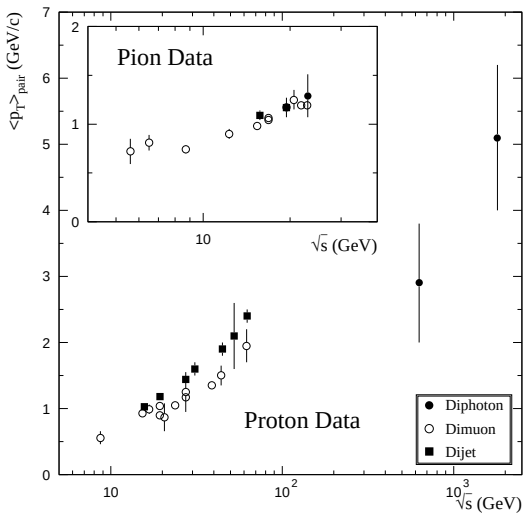

FIG. 30. The average p_T of pairs of muons, photons, and jets produced in hadronic collisions versus $\sqrt{s}$.

Perturbative QCD corrections are insufficient to explain the size of the observed k_T and full resummation calculations are required to explain Drell-Yan, W/Z and diphoton distributions. [26] These resummation calculations qualitatively describe the growth of the $< k_T >$ with center-of-mass energy. Currently, however, there is no rigorous k_T resummation calculation available for single photon production. The calculation is quite challenging in that the final state parton takes part in soft gluon emission and in color exchange with initial state partons, in contrast with the Drell-Yan and diphoton cases. Also, the calculation is complicated by the fact that several overlapping power-suppressed corrections can contribute and, at high x, threshold effects are important. Nevertheless, there has been recent theoretical progress. [27–29]

In lieu of a rigorous calculation of the resummed direct photon p_T distribution, the effects of soft gluon radiation can be approximated by a convolution of the NLO cross section with a Gaussian k_T smearing function. The value of $< k_T >$ to be used for each kinematic regime should be taken directly from relevant experimental observables, given the lack of a rigorous formalism, rather than from a theoretical prediction. The behavior of the k_T smearing

correction is quite different for the Tevatron collider and for fixed target experiments. In Figure 31 is shown the comparison of NLO theory calculations (with and without the k_T corrections)to the direct photon data from CDF and D0. The value of $< k_T >$ used (3.5 GeV/c) was taken directly from diphoton measurements at the Tevatron. [30] There are two points to note: (1) the agreement with the data is improved if the k_T correction is taken into account and (2) the k_T smearing effects fall off roughly as $1/p_T^2$. The latter behavior is the expectation for such a power-suppressed type of effect and is the behavior expected at the LHC, where the effects of the k_T smearing should not be important past p_T values of 30 GeV/c. [6]

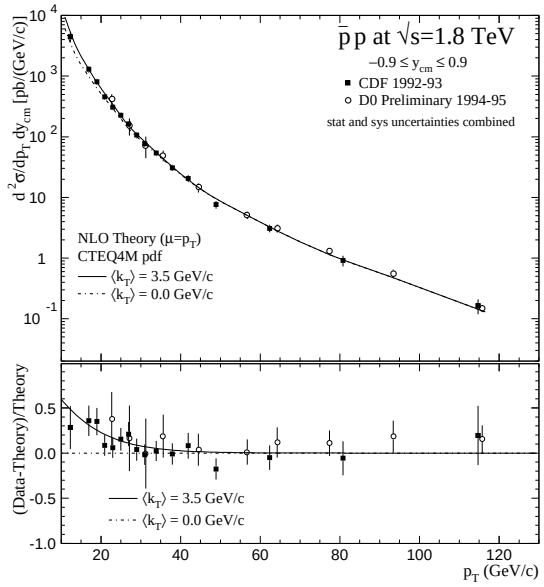

FIG. 31. The CDF and D0 isolated photon cross sections, compared to NLO QCD theory without k_T (dashed) and with k_T enhancement for $\langle k_T \rangle$ = 3.5 GeV/c (solid), as a function of p_T.

The k_T correction obtained for E706 at a center-of- mass energy of 31.6 GeV is shown in Figure 32.

---

[6]Similar k_T smearing effects should be present in all hard scattering cross sections, as for example, jet production at the Tevatron. The size of the experimental and theoretical systematic errors in the low E_T region make such a confirmation difficult.

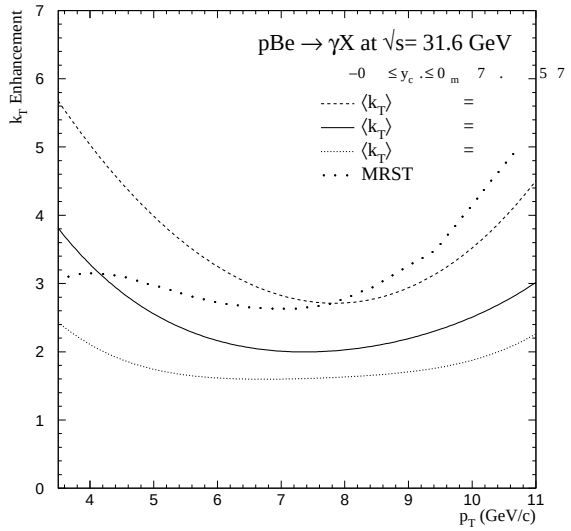

FIG. 32. The variation of k_T enhancements (ratio of cross sections with and without the k_T corrections) relevant to E706 direct photon data at 31.6 GeV, for different values of average k_T. In addition, the k_T correction for E706 used in the recent MRST fit is indicated.

The value of $< k_T >$ of 1.2 GeV/c was obtained from measurements of several kinematic observables in the experiment. [31] The k_T smearing effect is much larger here then observed at the collider and does not have the $1/p_T^2$ falloff. Also shown are the k_T corrrections using values of $< k_T >$ of 1.0 and 1.4 GeV/c (a reasonable estimate of the range of experimental uncertainty in the $< k_T >$ determination). Also shown is is k_T correction for the E706 data used in the recent MRST pdf's. The MRST k_T correction is larger which leads to a smaller gluon distribution in the relevant x range. (Both the CTEQ4 and MRST pdf's lead to good agreement with the E706 direct photon cross sections.) The differences between the k_T correction from Reference [31] and that from the MRST pdf's can be taken as an indication of the uncertainty in the value of this correction. The E706 direct photon and π^o cross sections at $\sqrt{s}$ =31.6 GeV are shown in Figure 33, along with the predictions with and without an additional Gaussian k_T smearing. Good agreement is observed with the nominal k_T correction of 1.2 GeV/c; however, the allowed range of variation of $\langle k_T \rangle$ (1.0-1.4 GeV/c) makes quantitative comparisons, and thus an extraction of the gluon distribution,

difficult. [7] Since the high p_T E706 data agrees well with CTEQ4M, it would thus disfavor the CTEQ4HJ pdf; as stated before, however, a definitive conclusion must await a more rigorous theoretical treatment.

A comparison of the gluon distributions in CTEQ4 and MRST is shown in Figure 34, along with the gluon distribution obtained from a fit to the k_T-corrected E706 direct photon data (along with DIS and DY data). The spread observed at high x emphasizes the conclusions discussed in the previous section.

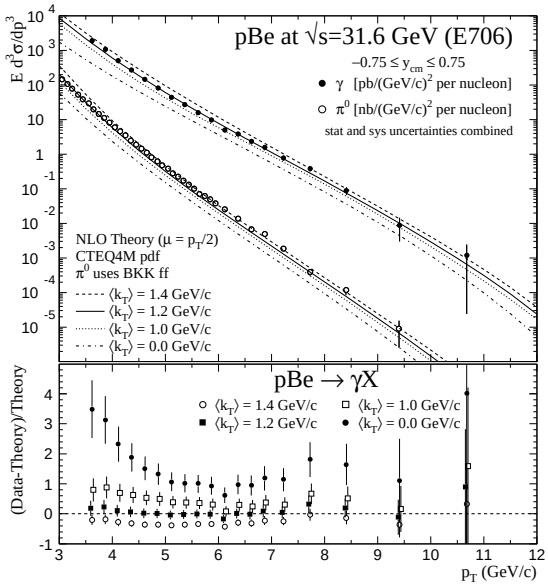

FIG. 33. The photon and π^o cross sections from E706 compared to k_T-enhanced NLO QCD calculations. In the bottom plot, the quantity (Data-Theory)/Theory is plotted, using k_T-enhanced calculations for several values of average k_T. The error bars have experimental statistical and systematic errors added in quadrature.

---

[7] NLO QCD predictions for fixed-target direct photon production also contain a non-negligible renormalization and factorization scale dependence; for example, changing the scale from $Q = p_T/2$ to $Q = p_T$ typically results in a decrease in the cross section of about 30%.

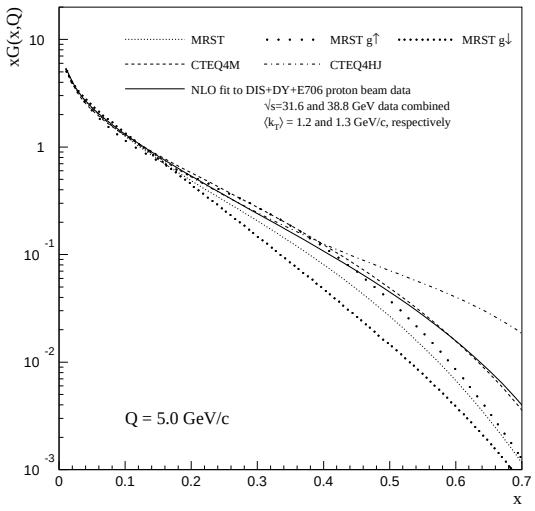

FIG. 34. A comparison of the CTEQ4M, MRST and CTEQ4HJ gluons and the gluon distribution derived from fits that use the E706 data. The $g\uparrow$ and $g\downarrow$ gluon densities correspond to the maximum variation of $\langle k_T \rangle$ that MRST has allowed in their fits.

B. Influence of Jets

An important process that is sensitive to the gluon distribution is jet production in hadron-hadron collisions. Processes responsible for jet production include gluon-gluon, gluon-quark and quark-quark(or anti-quark) scattering. In leading order, the jet cross section is proportional to $\alpha_s^2 g(x,Q)g(x',Q)$ and $\alpha_s^2 g(x,Q)q(x',Q)$. Precise data on jet production at the Fermilab Tevatron are now available over a wide range of transverse energy, and the theoretical uncertainties in most of this range are well-understood. Thus, it is to be expected that jet production can provide a good constraint on the gluon distribution

The jet data that has been utilized in global pdf fits has been from the CDF and D0 collaborations. [8] The data cover a wide kinematic range (E_T values from 15 to 450 GeV/c

[8]The experimental and theoretical errors associated with the UA2 jet cross section make its use

corresponding to an x range of .02 to 0.5). The CDF jet data from Run IA were utilized in the CTEQ4HJ pdf fit. [32] In the CTEQ4HJ fit, a large emphasis was given to the high E_T data points which show a deviation from NLO QCD predictions with "conventional" pdf's. Given the lack of constraints on the high x gluon distribution discussed in Section VI, the extra emphasis on the high E_T region was enough to cause a significant increase in the gluon distribution; for example, the gluon distribution at an x value of 0.5 (Q=100 GeV) increases by a factor of 2. Since the dominant jet subprocess in this region is $\overline{q}q$ scattering (see Figure 35), the increase in the gluon distribution of a factor of 2 causes only a 20% increase in the jet cross section. This is sufficient to pass through the bottom of the CDF high E_T jet error bars. (See Figure 36.) The preliminary jet cross sections from Run 1B(90 $pb^{-}1$) from both the CDF and D0 experiments were used in the CTEQ4M fits, but with statistical errors only and only for the E_T range of 50-200 GeV/c. The lower E_T points have substantial systematic errors on both the theoretical and experimental sides and the higher E_T points contain the CDF excess at high E_T. The inclusion of the jet data serves to considerably constrain the gluon distribution over the x range of 0.1 to 0.2. The resulting gluon (CTEQ4M) does not decrease the excess observed in CDF at high E_T.

---

in pdf fits difficult.

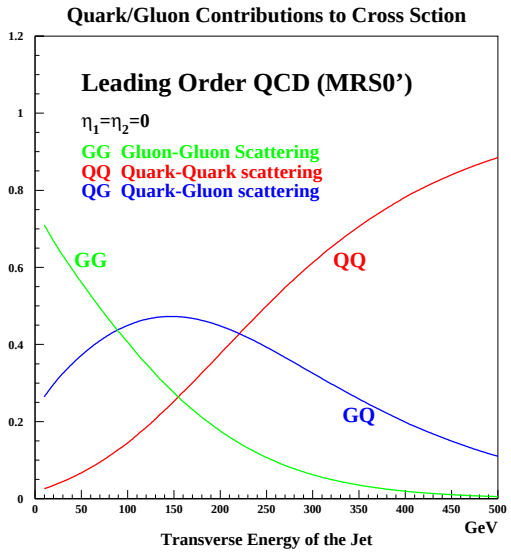

FIG. 35. The relative proportion of processes contributing to jet production at the Tevatron ($\overline{p}p$ at 1.8 TeV).

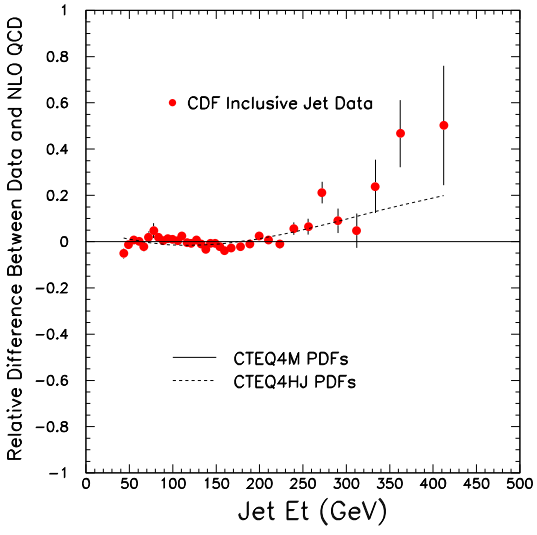

FIG. 36. A comparison of the preliminary CDF jet cross section from Run 1b to NLO predictions using the CTEQ4M and CTEQ4HJ pdf's.

The published D0 jet cross section [33] along with the (soon-to-be published) CDF jet cross section [34] from Run 1B were used in the recently released CTEQ5 parton distribu-

tions. The fits use the full E_T range for the cross sections and use the correlation information on the systematic errors as contained in the covariance matrices for both experiments. As can be seen in Figure 37, the two experiments are in agreement with each other except for a slight normalization shift [9]; the two highest E_T data points for CDF are above those for D0, but both experiments have large statistical errors in this region. As can be seen in Figure 38 and Figure 39, the NLO QCD prediction with the CTEQ5M pdf is in good agreement with both experiments. A comparison of the CTEQ5M gluon to that from CTEQ4M is shown in Figure 40 for three different Q values. The CTEQ5M gluon is very similar to CTEQ4M, except perhaps at very high x. The CTEQ4HJ pdf has been updated to complement the new CTEQ5M pdf. A comparison of the CTEQ5M and CTEQ5HJ gluon distributions (at 3 different Q values) is shown in Figure 41. The CTEQ5HJ pdf gives almost as good a global fit as CTEQ5M to the full set of data on DIS and DY processes, and has the feature that the gluon distribution is significantly enhanced in the high x region, thus resulting in improved agreement with the observed trend of jet data at high E_T.

A comparison of the CTEQ5 and MRST gluon distributions is shown in Figure 42 at a Q value of 5 GeV. A comparison of the NLO QCD predictions for the CDF and D0 inclusive jet cross sections using CTEQ5M, CTEQ5HJ and the MRST1,2 and 3 pdf's are shown in Figures 43 and 44, respectively. Note that the MRST2 pdf (gluon up; no k_T correction applied to the direct photon data) leads to good agreement with the CDF and D0 jet cross sections, once a small normalization factor is used.

---

[9] A shift on the order of 3% is expected since the two experiments use values for the total inelastic cross section that differ by that amount.

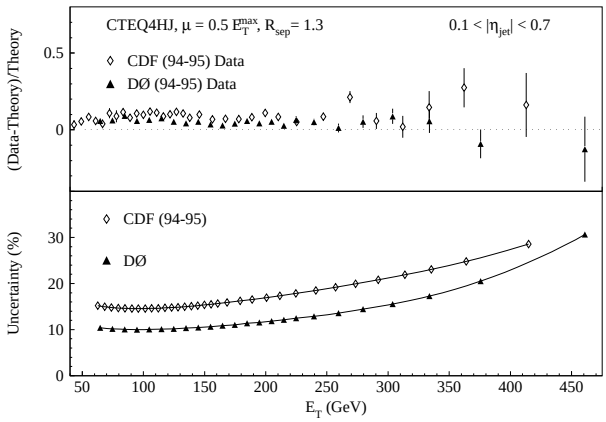

FIG. 37. A direct comparison of the inclusive jet cross sections from Run 1b from CDF and D0 for the rapidity range from 0.1 to 0.7.

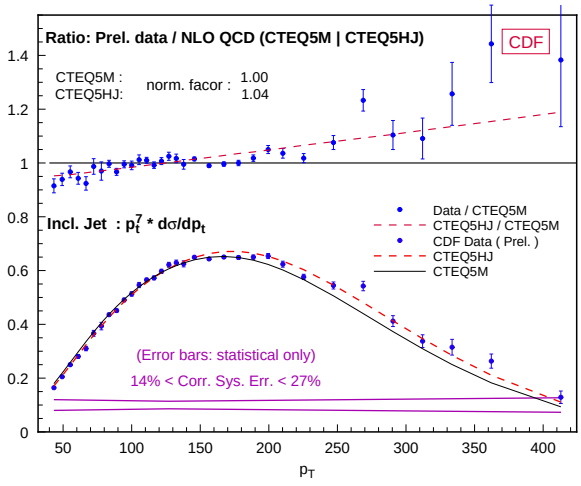

FIG. 38. A comparison of the Run 1B CDF inclusive jet cross section to the CTEQ5 fits. The bottom plot shows the measured cross section multiplied by p_T^7 in order to allow a linear display. The top plot shows the ratio of the measured cross section to that calculated with CTEQ5M, as well as the ratios of CTEQ5HJ to CTEQ5M.

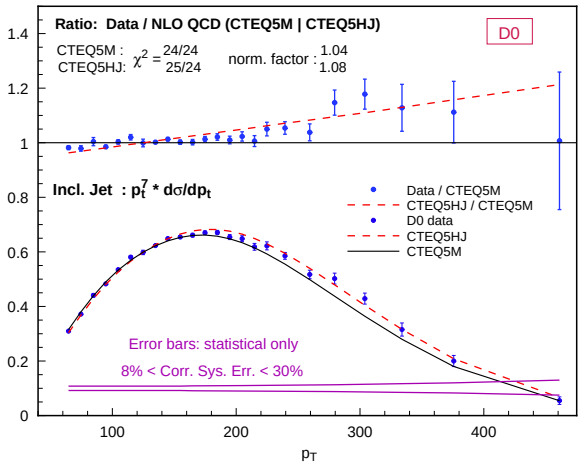

FIG. 39. A comparison of the Run 1B D0 inclusive jet cross section to the CTEQ5 fits with same parameters as the CDF jet figure.

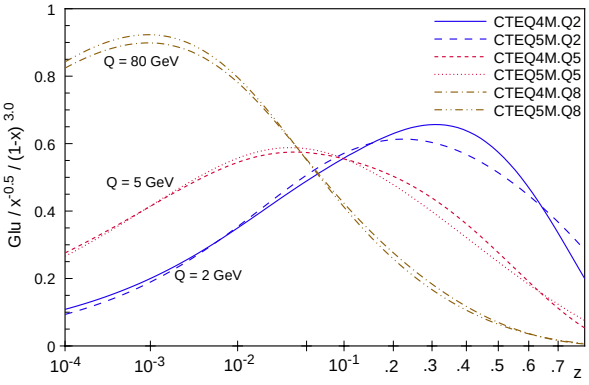

FIG. 40. A comparison of the CTEQ4M and CTEQ5M gluon distributions at 3 different Q values.

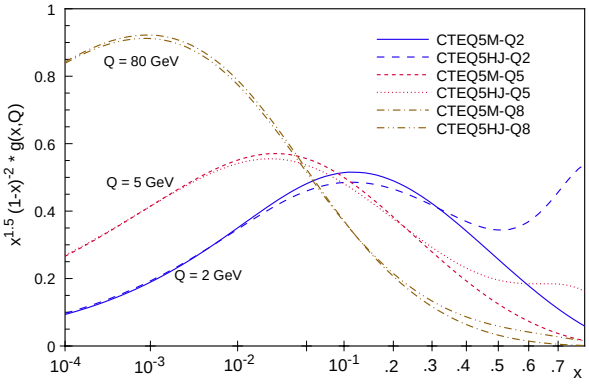

FIG. 41. A comparison of the CTEQ5M and CTEQ5HJ gluon distributions at 3 different Q values. Note the effect of QCD evolution.

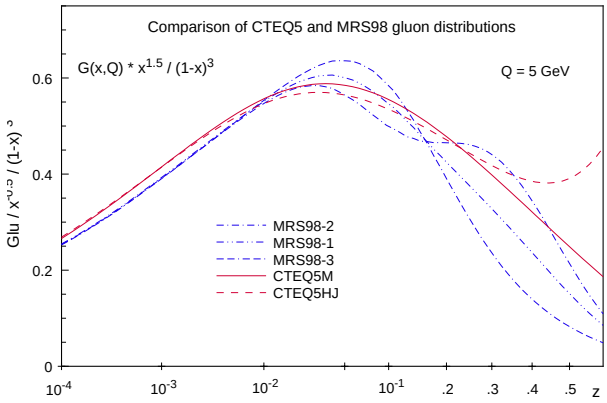

FIG. 42. A comparison of the CTEQ5M, CTEQ5HJ and MRST1,2, and 3 gluon distributions at a Q value of 5 GeV. The distributions are multiplied by a factor of $x^{1.5}/(1-x)^3$ in order to be plotted on a linear scale.

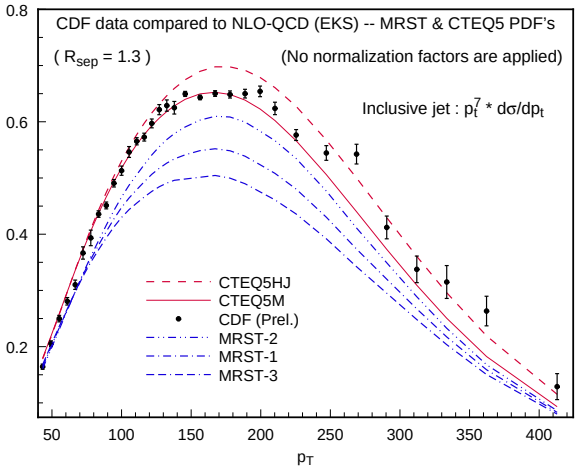

FIG. 43. A comparison of the CTEQ5M, CTEQ5HJ and MRST1,2 and 3 pdf predictions for the inclusive jet cross section for the CDF Run 1B data. The cross section is multiplied by a factor of p_T^7 in order to enable it to be plotted on a linear scale.

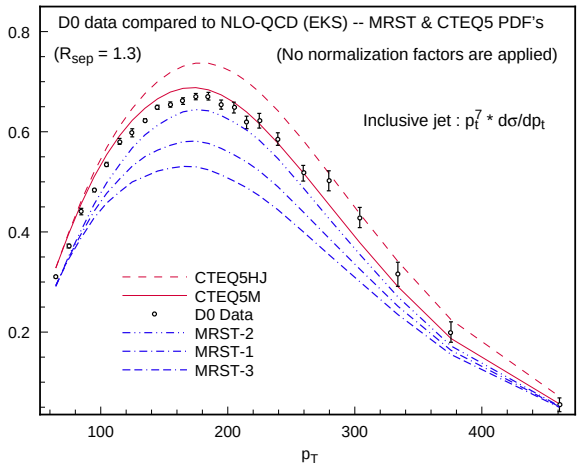

FIG. 44. A comparison of the CTEQ5M, CTEQ5HJ and MRST1,2 and 3 pdf predictions for the inclusive jet cross section for the D0 Run 1B data. The cross section is multiplied by a factor of p_T^7 in order to enable it to be plotted on a linear scale.

VIII. PROGRESS BEFORE THE LHC TURNS ON

DGLAP-based perturbative QCD calculations have been extremely successful in describing data in DIS, DY and jet production, as well as describing the evolution of parton distributions over a wide range of x and Q^2. From the pdf point-of-view, the primary problem lies in the calculation of fixed target direct photon cross sections; they can serve as a primary probe of the gluon distribution at high x. However, rigorous theoretical treatment of soft gluon effects (requiring both k_T and Sudakov resummation) will be required before the data can be used with confidence in pdf fits.

Differential dijet data from the Tevatron explore a wider kinematic range than the inclusive jet cross section, as shown in Figure 45. Both CDF and D0 have dijet cross section measurements from Run I which may also serve probe the high x gluon distribution, in regions where new physics is not expected but where any parton distribution shifts should be observable. The ability to perform such cross-checks is essential.

CDF and D0 will accumulate on the order of 2-4 fb^{-1} of data in Run II (from 2000-2003), a factor of 20-40 greater than the current sample. This sample should allow for more

detailed information on parton distributions to be extracted from direct photon and DY data, as well as from jet production. Run III (2003-2007) offers a data sample potentially as large as $30 fb^{-1}$.

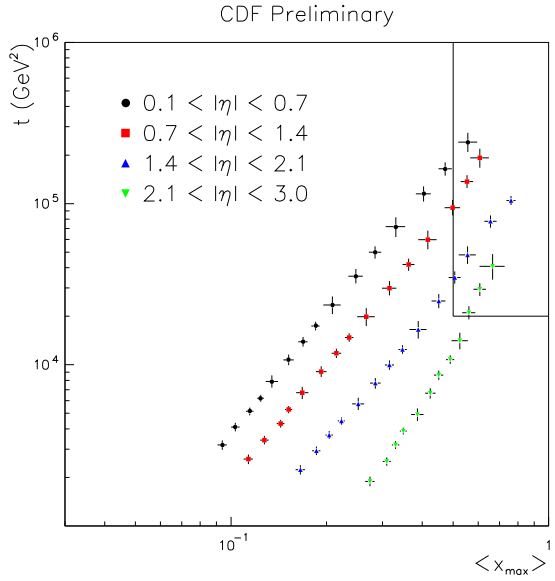

FIG. 45. A plot of the $\hat{t}$ vs x_{max} reach for the CDF differential dijet cross analysis in Run 1B. The box in the upper right hand corner indicates the kinematic region where a possible excess at HERA has been probed.

H1 and ZEUS will continue the analysis of the data taken with positrons in 1991-97. HERA switched to electron running in 1998 and plans to deliver approximately 60 pb^{-1} in 1999-2000. In 2000, the HERA machine will be upgraded for high luminosity running, with yearly rates of 150 pb^{-1} expected, allowing for an integrated luminosity of about 1 fb^{-1} by 2005. This will allow for an error of a few percent on the structure function F_2 for Q^2 scales up to $10^4 GeV^2$. The gluon density, derived from scaling violations of F_2, should be known to an accuracy of less than 3% in the kinematic range $10^{-4} < x < 10^{-1}$.

IX. DESCRIPTION OF CURRENT PDF'S

In the last few years, improved and new experimental data have become available in many processes; these data have been incorporated into the new CTEQ and MRS analyses.

- Deep inelastic scattering: The NMC and CCFR collaborations have published final analyses of their respective data on muon-nucleon and neutrino-nucleus scattering. These new results have led to subtle changes in their implications on α_s and parton distribution determination. H1 and ZEUS have published more extensive and precise data on the total inclusive structure function F_2^p. These new results provide tighter constraints on the quark distributions as well as on the gluon distribution (through the Q^2 evolution of the structure functions). The HERA experiments have also presented new data on semi-inclusive F_2^c, with charm particles in the final state.

- Lepton-pair production (p/d) asymmetry: The E866 collaboration has measured the ratio of lepton-pair production (DY) in pp and pd collisions over the x range of (0.03-0.35), thus greatly expanding the experimental constraint on the ratio of parton distributions $\overline{d}/\overline{u}$ from the single point of NA51.

- Lepton charge asymmetry in W production: The CDF collaboration has improved the accuracy and extended the y range of the measurement of the asymmetry between $W \to l^{\pm}\nu$ at the Tevatron. This provides additional constraints on d/u.

- Inclusive large p_T jet production: CDF and D0 have recently finished their final analysis of the Run IB inclusive jet cross data, including full information on the correlated systematic errors. The availability of systematic errors are important for the global analysis, since they dominate the experimental uncertainty over much of the measured p_T range. This jet data provides crucial constraints on the gluon distribution in the CTEQ5 global analysis.

The CTEQ5 pdf release contain six sets of parton distribution functions:

- CTEQ5M: the main pdf set where the fit was performed in the $\overline{MS}$ scheme

- CTEQ5D: the set derived from a fit in the DIS scheme

- CTEQ5L: the set derived from a leading order fit

- CTEQ5HJ: performed in the $\overline{MS}$ scheme, but with an increased emphasis to the CDF high E_T data points
- CTEQ5HQ: uses a systematic generalization of the conventional $\overline{MS}$ scheme to include heavy-quark partons
- CTEQ5F3: uses a fixed 3-flavor scheme where charm and bottom quarks are treated as heavy particles and not partons

The MRST pdf's contain 5 sets of parton distribution functions repeated in 4 separate schemes:

- MRST(1): the main pdf performed in the $\overline{MS}$ scheme with the nominal $\alpha_s(M_Z)(.1175)$ and k_T-smearing values
- MRST(2): as in MRST(1) but with smaller direct photon k_T-smearing corrections and thus a larger gluon distribution
- MRST(3): as in MRST(1) but with larger direct photon k_T-smearing corrections and thus a smaller gluon distribution
- MRST(4): as in MRST(1) but with a lower value of $\alpha_s(M_Z)$ (.1125)
- MRST(5): as in MRST(1) but with a higher value of $\alpha_s(M_Z)$ (.1225)
- MRSTDIS(1-5): DIS scheme versions of MRST(1-5)
- MRSTLO(1-5): LO scheme versions of MRST(1-5)
- MRSTHT(1-5): HT versions of MTST(1-5)

X. PHYSICS CROSS SECTIONS AT THE LHC AND THE ROLE OF LHC DATA IN PDF DETERMINATION

ATLAS measurements of DY (including W and Z), direct photon, jet and top production will be extremely useful in determining pdf's relevant for the LHC. The data can be input

to the global fitting programs, where it will serve to confirm/constrain the pdf's in the LHC range. Again, DY production will provide information on the quark (and anti-quark) distributions while direct photon, jet and top production will provide, in addition, information on the gluon distribution.

The isolated [10] direct photon cross section at the LHC is shown in Figure 46, along with the predictions of the MRST and CTEQ4M pdf's. [5] In the region plotted, the dominant subprocess is gluon-Compton scattering ($gq \to \gamma q$). Note that the two pdf's lead to similar predictions in this x range.

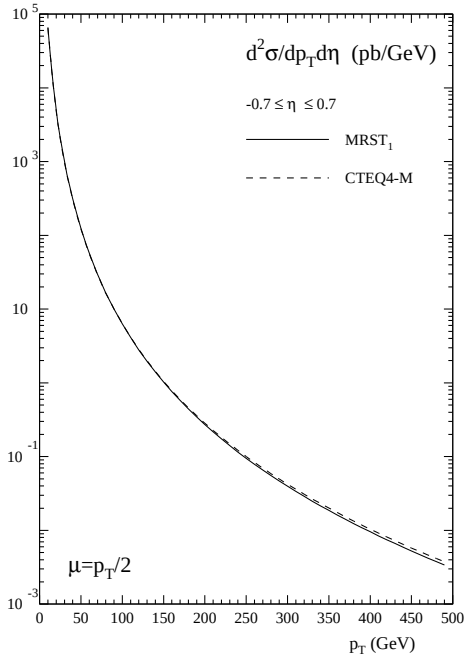

FIG. 46. The isolated direct photon cross section at the LHC along with the NLO QCD predictions using the CTEQ4M and MRST pdf's.

The resummed NLO cross section (using the CTEQ4 pdf) for the production of diphotons at the LHC is shown in Figure 47 plotted as a function of the diphoton mass and broken down by subprocess. [35] For relatively low diphoton masses ($< 60\ GeV/c^2$), the gg scattering subprocess is dominant and continues to be appreciable out to diphoton masses greater than

[10] Using isolation cuts similar to those used by CDF and D0.

100 GeV/c^2. One point to note is that the resummed gg calculation uses an approximate form for the $gg \to \gamma\gamma g$ matrix element. An implementation of the exact form will increase the contribution of the gg subprocess at higher diphoton masses. [37] Measurements of diphoton production at the LHC will contribute to an improved knowledge of the relevant parton pdf's and parton-parton luminosity functions for the production of the Higgs (which is largely due to gg scattering for low to moderate Higgs' masses).

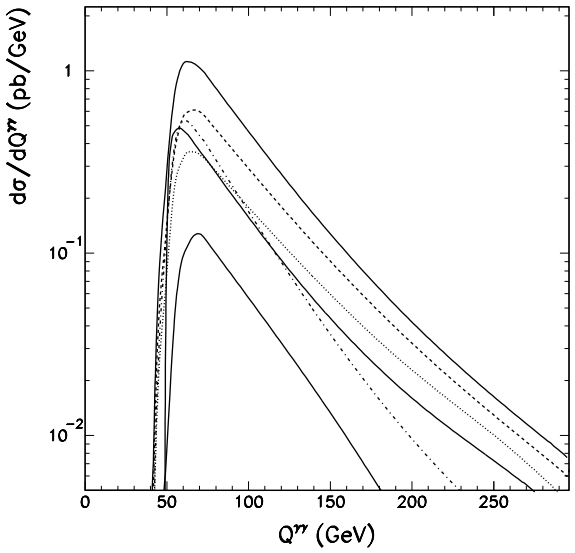

FIG. 47. The invariant mass distribution of photon pairs at the LHC. The total resummed contribution (upper solid), and the resummed $q\overline{q} + qg \to \gamma\gamma X$ (dashed), $q\overline{q} \to \gamma\gamma g$ (dash-dotted), as well as the fragmentation (lower solid) contributions are shown separately. The $q\overline{q} \to \gamma\gamma$ leading order result is shown in the middle solid curve. A p_T cut of 25 GeV/c has been applied to each photon, along with a rapidity cut of 2.5 and a requirement that the leading photon has less than 70% of the p_T of the photon pair.

For comparison purposes, the diphoton cross section at the Tevatron is shown, plotted in a similar manner, and compared to the CDF data from Run 1B. [36] For masses less than 30 GeV/c^2, the gg subprocess dominates and remains appreciable out to mass values of 50 GeV/c^2 or so. The same comment about the approximate form for the $gg \to \gamma\gamma g$ matrix element applies here also. Note that the much higher statistics for Run II will allow both the

gg luminosity and the physics formalism for diphoton production to be probed with much higher statistics.

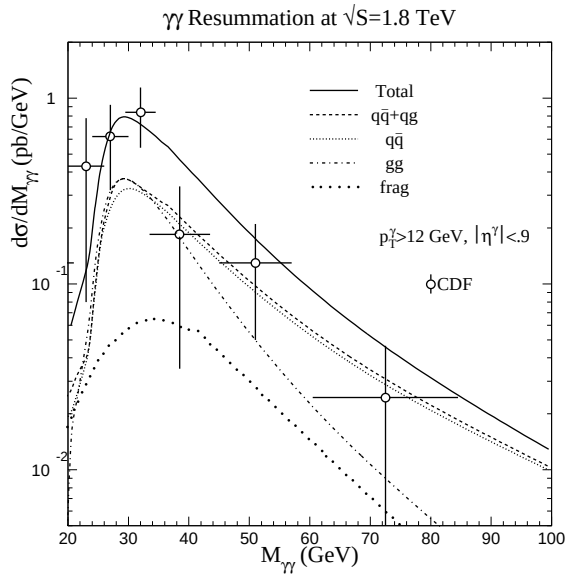

FIG. 48. The predicted distribution for the invariant mass of the photon pair from the resummed calculation compared to the CDF data, with the CDF cuts imposed in the calculation.

The subprocesses responsible for jet production at the LHC are similar to the subprocess plot for the Tevatron. The relative fraction of each subprocess is very close to the fraction at the Tevatron, if the fractions are plotted as a function of x_T. Gluon-gluon scattering dominates at the lowest values of E_T, with gluon-quark dominating at moderate values of E_T and quark-quark at the highest values.

A comparison of jet production at the Tevatron and the LHC is shown in Figure 49. [5] The "reach" at the LHC is to jet E_T values of approximately 4 TeV/c. There are noticable differences between the predictions using the 3 pdf's listed. This difference is more evident in the linear comparison shown in Figure 50. [5] An E_T value of 4 TeV/c corresponds to an x_T value of about 0.57. At this x_T value, the CTEQ4HJ pdf prediction is about 30% higher than the CTEQ4M prediction, while the MRST prediction is about 7% smaller. Note that the size of the relative deviations is very similar at the LHC and Tevatron.

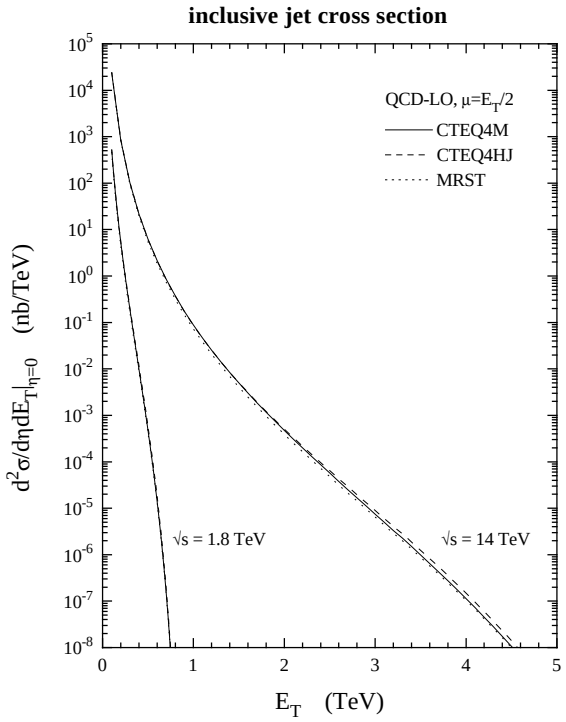

FIG. 49. The inclusive jet cross sections at a rapidity of 0 for both the Tevatron and the LHC.

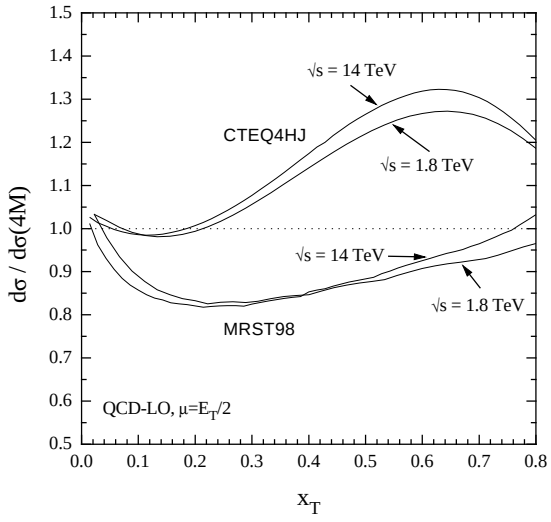

FIG. 50. A comparison of the predictions for the inclusive jet cross sections at a rapidity of 0 for both the Tevatron and the LHC using three different pdf's.

The cross sections for the production of W^+ and W^- at the LHC are symmetric with respect to $\eta = 0$. This is in contrast to the asymmetry that is observed at the Tevatron due to $\overline{p}p$ collisions rather than pp collisions. The W^+ production cross section is larger than the W^- production cross section at the LHC; in addition there is a great deal of information on parton distribution densities that can be obtained from the $W^{+,-}$ rapidity distributions. For example, in Figure 51, the $W^{+,-}$ rapidity distributions are shown along with the parton kinematics probed at rapidites of 0 and 3. [5]

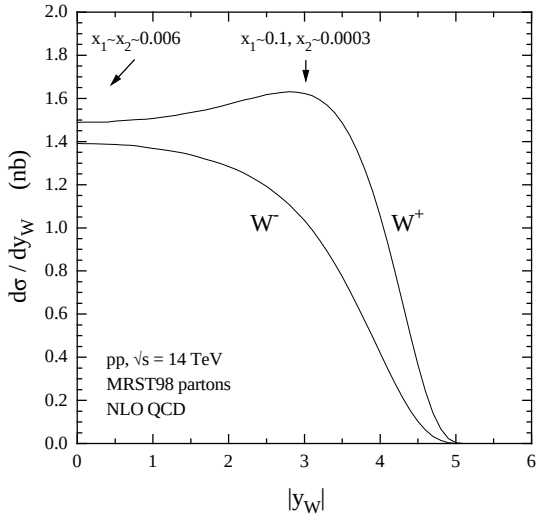

FIG. 51. The $W^{+,-}$ rapidity distributions for pp collisions at the LHC.

Another possibility that has been suggested is to directly determine parton-parton luminosities (and not the parton distributions per se) by measuring well-known processes such as W/Z production. [38] This technique would not only determine the product of parton distributions in the relevant kinematic range but would also eliminate the difficult measurement of the proton-proton luminosity. It may be more pragmatic, though, to continue to separate out the measurements of parton pdf's (though global analyses which may contain LHC data) and of the proton-proton luminosity. The measurement of the latter quantity can be pegged to well-known cross sections, such as that of the W/Z, as has been suggested for the Tevatron.

XI. RESOURCES AVAILABLE

The pdf's and relevant information can be obtained from the CTEQ and MRS groups at the following web addresses. In addition, there are other sites where parton distributions are collected, one of which is shown below.

MRS: http://durpdg.dur.ac.uk/HEPDATA/MRS.html

CTEQ: http://www.phys.psu.edu/~cteq/

POTPOURRI OF PARTONS: http://www.phys.psu.edu/~cteq/

In addition, specialized pdf fits (and the resulting parton distributions) within the CTEQ framework are possible for ATLAS use. [11]

For a recent review of Tevatron and HERA QCD results, see Reference [39].

XII. ACKNOWLEDGEMENTS

I would like to thank James Stirling and Lenny Apanasevich for providing many of the figures and to James Stirling, Steve Mrenna and my CTEQ colleagues for useful comments.

---

[1] H.L. Lai, J. Huston et al., **hep-ph/9903282**.

[2] A.D. Martin, R.G. Roberts, W.J. Stirling and R. Thorne, *Eur. Phys. J.***C4**, 463 (1998)

[3] See, for example, the plenary talk given by Y. Dokshitzer at the ICHEP conference in Vancouver, **hep-ph/9812252**.

[4] M. Bonesini et al., *Z. Phys.* **C38**, 371(1988); *ibid.* **C37**,535(1988); *ibid.* **C37**, 39.

[5] I would like to thank James Stirling for providing these plots; most were taken from his talk on LHC physics at the Feb 1998 workshop on LHC Physics Processes.

---

[11] Contact J. Huston at huston@pa.msu.edu.

[6] S. Kuhlmann, W.-K. Tung and H. L. Lai, *Phys. Lett.* **409B**, 271 (1997)

[7] M. Gluck, E. Reya, A. Vogt, *Eur. Phys. J.***C5**, 461 (1998).

[8] G. Marchesini et al., **hep-ph/9607393**.

[9] T. Sjostrand, **hep-ph/9508391**.

[10] A.D. Martin, R.G. Roberts, W.J. Stirling and R. Thorne, *Phys. Lett.***B443**, 301 (1998).

[11] J. Botts et al., *Phys. Lett.***304B**, 159 (1993).

[12] CTEQ internal report (unpublished).

[13] H.L. Lai, J. Huston et al., *Phys. Rev.***D51**, 4763 (1995).

[14] H.L. Lai, J. Huston et al., *Phys. Rev.***D55**, 1280 (1997), **hep-ph/9606399**.

[15] W. J. Stirling, private communication.

[16] W.T. Giele, Stephane Keller, *Phys. Rev.***D58**, (1998), **hep-ph/9803393**.

[17] S. Alekhin, **hep-ph/9166213**, submitted to Elsevier Science.

[18] CDF Collaboration, F. Abe et al., *Phys. Rev. Lett.***81**, 5754 (1998), **hep-ex/9809001**.

[19] A. Baldit et al., *Phys. Lett.***332B**, 244 (1994).

[20] E.A. Hawker et al., *Phys. Rev. Lett.* **80**, 3715 (1998), **hep-ex/9803011**.

[21] W. G. Seligman et al., *Phys. Rev. Lett.***79**, 1213 (1997).

[22] U.K. Yang, A. Bodek, **hep-ph/9809480**, submitted to *Phys. Rev. Lett.*

[23] J. Huston et al., *Phys. Rev.***D58** (1998), **hep-ph/9801444**.

[24] J. Huston et al., *Phys. Rev.***D51**, 6139 (1995), **hep-ph/9501230**.

[25] P. Aurenche et al., **hep-ph/9811382**.

[26] C. Balazs, C.-P. Yuan, *Phys. Rev.***D56**, 5558 (1997) and references therein.

[27] E. Laenen, G. Oderda, G. Sterman, *Phys. Lett.***438B**, 173(1998), **hep-ph/9806467**.

[28] S. Catani, M. Mangano, P. Nason, **hep-ph/9806487**.

[29] H-n. Li, hep-ph/9812363; H-n. Li, **hep-ph/9811340**.

[30] See, for example, the talk of S. Linn at the ICHEP conference in Vancouver.

[31] L. Apanasevich, J. Huston et al., *Phys. Rev. Lett.***59** (1999), **hep-ph/9808467**.

[32] J.Huston et al., *Phys.Rev.Let.***77**, 444(1996).

[33] B. Abbott et al., **hep-ex/9807018**.

[34] F. Bedeschi, talk at 1999 Hadron Collider Physics Conference, Bombay, India, January, 1999.

[35] C. Balazs et al., **hep-ph/9810319**, accepted by *Phys. Rev.*D.

[36] C. Balazs et al., *Phys. Rev.***D57**, 6934(1998), **hep-ph/9712471**.

[37] C. Balazs, private communication.

[38] M. Dittmar, F. Pauss, D. Zuercher, *Phys. Rev.***D56**, 7284; **hep-ex/9705004**.

[39] J. Huston, plenary talk on QCD at the ICHEP conference in Vancouver ("QCD at High Energies"); **hep-ph/9901352).**